

# Reason Like a Radiologist: Chain-of-Thought and Reinforcement Learning for Verifiable Report Generation

Peiyuan Jing<sup>\*1</sup> KinHei Lee<sup>\*1</sup> Zhenxuan Zhang<sup>\*1</sup> Huichi Zhou<sup>1</sup> Zhengqing Yuan<sup>2</sup> Zhifan Gao<sup>3</sup> Lei Zhu<sup>4</sup>  
Giorgos Papanastasiou<sup>5</sup> Yingying Fang<sup>1</sup> Guang Yang<sup>1</sup>

## Abstract

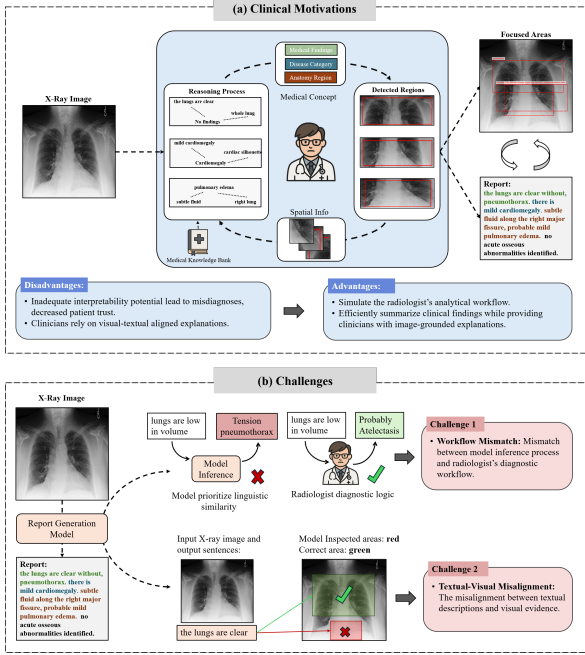
Radiology report generation is critical for efficiency but current models lack the structured reasoning of experts, hindering clinical trust and explainability by failing to link visual findings to precise anatomical locations. This paper introduces BoxMed-RL, a groundbreaking unified training framework for generating spatially verifiable and explainable radiology reports. Built on a large vision-language model, BoxMed-RL revolutionizes report generation through two integrated phases: (1) In the Pretraining Phase, we refine the model via medical concept learning, using Chain-of-Thought supervision to internalize the radiologist-like workflow, followed by spatially verifiable reinforcement, which applies reinforcement learning to align medical finding with bounding box. (2) In the Downstream Adapter Phase, we freeze the pretrained weights and train a downstream adapter to ensure fluent and clinically credible report. This framework precisely mimics radiologists' workflow, compelling the model to connect high-level medical concepts with definitive anatomical evidence. Extensive experiments on public datasets demonstrate that BoxMed-RL achieves an average 7% improvement in both METEOR and ROUGE-L metrics compared to state-of-the-art methods. An average 5% improvement in large language model-based metrics further underscores BoxMed-RL's robustness in generating high-quality radiology reports.

## 1. Introduction

Radiological imaging plays a crucial role in clinical decision-making by significantly aiding disease diagnosis and patient management. The explainability and transparency of medical reports generated from radiological images are essential (Brady et al., 2012; Goergen et al., 2013). Inadequate explainability can lead to miscommunications among clinicians, potential misdiagnoses, decreased patient trust, and ultimately compromised patient safety (Satia et al., 2015). Clinicians rely on visual explanations to understand not only the diagnostic outcome but also the anatomical and pathological reasoning behind these conclusions (Pan et al., 2025). This requires models to align visual perception in images, such as identifying lesions, anatomical landmarks, and spatial relationships with clinical language (Rajpurkar & Lungren, 2023). The rapidly increasing volume of radiological images produced annually has created substantial workload pressures on radiologists, complicating thorough image interpretation and increasing the risk of diagnostic inaccuracies (Delrue et al., 2011). This issue has led to significant backlogs in radiological reporting, particularly within public healthcare systems, further intensifying the risk of medical errors and inefficient use of medical resources (Wang et al., 2022a; Yang et al., 2023; Gao et al., 2024). Therefore, there is a need for an explainable automated medical report generation model that combines fine-grained visual perception with clinical reasoning to generate reports (Fig. 1 (a)). Such tools require the ability to precisely localize and interpret visual findings (e.g., tumors, fractures, or tissue anomalies) while explicitly linking these observations to diagnostic conclusions in natural language. By doing so, they can efficiently summarize clinical findings while providing clinicians with transparent, image-grounded explanations that simulate the radiologist's analytical workflow (Tang et al., 2025).

Despite progress in automated medical report generation, existing methods face critical limitations in producing clinically trustworthy explanations (Wang et al., 2023b; Tanida et al., 2023). As shown in Fig. 1 (b), two core challenges are: (1) The mismatch between model inference process and radiologists' diagnostic workflows. (2) The misalignment

<sup>\*</sup>Equal contribution <sup>1</sup>Imperial College London, London, UK <sup>2</sup>University of Notre Dame, USA <sup>3</sup>Shenzhen Campus of Sun Yat-sen University, China <sup>4</sup>HKUST(GZ), China <sup>5</sup>Athena Research Centre, Athens. Correspondence to: Guang Yang <g.yang@imperial.ac.uk>.



**Figure 1.** The motivation and challenges of our BoxMed-RL. (a) Clinical motivation: Radiologists interpret chest X-rays by combining spatial information with medical knowledge to identify findings, associate them with disease categories, and localize them in anatomical regions. (b) Challenges: Two major limitations are Workflow Mismatch and Textual-Visual Misalignment.

between textual descriptions and visual evidence. First, most methods generate free-form narratives that deviate from radiologists’ structured diagnostic logic (e.g., systematically analyzing anatomical regions to rule out differential diagnoses) (Rajpurkar & Lungren, 2023). These models lack the hierarchical reasoning ability to think like a radiologist, for example, they may state contradictory findings like “lungs are low in volume” followed by “tension pneumothorax” (which typically causes increased lung volume) (Pan et al., 2025). Such errors arise because models prioritize linguistic similarity over clinical plausibility, failing to mimic the structured reasoning workflow of radiologists. Second, existing systems often fail to correlate their statements with visual evidence (e.g., noting a “lung nodule” without localizing it) (Yang et al., 2022; Wang et al., 2022b). This creates ambiguity, as clinicians cannot verify whether findings (e.g., “normal pulmonary vasculature”) are derived from image patterns or inferred from biased language priors (Zhang et al., 2024c; Tanida et al., 2023). For instance, a model might correctly describe “a lung nodule in the right upper lobe” but point to the left lung during inference. This occurs because current methods lack the ability to truly interpret medical images; instead, they rely on tokenized visual representations, which only capture implicit vision-language correlations rather than explicit anatomical understanding.

As a result, models are allowed to “guess” plausible findings without spatial fidelity. These limitations erode clinician trust and risk misdiagnosis, as ungrounded or illogical explanations hinder clinical verification and workflow integration. (Satia et al., 2015; Zhang et al., 2024d)

Although recent methods have advanced report generation, they still struggle to resolve workflow mismatch and textual-visual misalignment (Chen et al., 2020; Liu et al., 2021a). Traditional encoder-decoder models (Fig. 2 (a)), such as R2Gen (Chen et al., 2020) and GSK (Yang et al., 2022), directly map input images to free-form reports, overlooking spatial relationships between findings and anatomical regions. This architectural simplicity makes them insensitive to fine-grained image details, often producing generic descriptions (e.g., “lung opacity”) without specifying pathologies (e.g., “right middle lobe consolidation”). Region-enhanced encoder-decoder models (Fig. 2 (b)), including MA (Wang et al., 2022a) and CMN (Chen et al., 2021), partially address this by integrating regional features (e.g., lesion patches or organ-level segments) into the encoder. Although this improves localized pattern awareness, their rigid encoder-decoder architecture inherently lacks reasoning ability, for instance, failing to prioritize critical findings (e.g., masses) over benign ones (e.g., calcifications) during inference. Prompt-driven large language models (Fig. 2 (c)), such as STREAM (Yang et al., 2025) and R2GenGPT (Wang et al., 2023a), leverage textual and visual prompts to guide report generation using region information. However, they force spatial data (e.g., bounding boxes) to be tokenized into embeddings, making their inability to directly process visual inputs, losing textual-visual fidelity. While large language models exhibit generic reasoning capabilities, they fail to replicate radiologist’s structured diagnostic workflow (e.g., systematically analyzing anatomical regions to rule out diagnoses), producing free-form narratives lacking clinical coherence. These architectures share two critical flaws: All architectures lack hierarchical diagnostic logic (e.g., from findings to anatomy), producing reports that omit differential analysis or systematic workflows. They treat vision and language as loosely coupled modalities, neglecting to enforce spatially explicit alignment (e.g., linking “left lung nodule” to bounding boxes). These flaws result in reports that are ambiguous or misaligned with diagnostic logic, risk misdiagnosis, and erode clinician trust (Sloan et al., 2024; Zhang et al., 2024d; Satia et al., 2015; Nan et al., 2024).

To address these critical challenges, we propose BoxMed-RL (Fig. 2 (d)), an innovative two-phase training framework designed to enhance explainability and clinical trustworthiness in automated medical report generation. Compared to previous methods that rely on free-form generation or implicit textual-visual correlations, we explicitly incorporate structured medical reasoning and spatially verifiable learning, ensuring radiologist-like workflow and precise

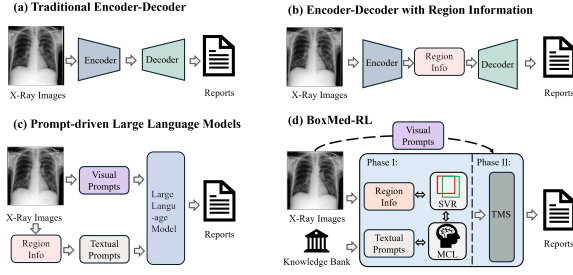


Figure 2. Comparison of medical report generation architectures. (a) Traditional encoder-decoder framework. (b) Region-enhanced encoder-decoder models. (c) Prompt-driven large language models. (d) Our proposed BoxMed-RL.

alignment between generated descriptions and anatomical evidence. BoxMed-RL advances explainable report generation through two key innovations in its Pretraining Phase: (1) Medical Concept Learning (MCL), a module to internalize the diagnostic flow of radiologist. This enables models to assimilate and replicate radiologists’ structured diagnostic reasoning. (2) Spatially Verifiable Reinforcement (SVR), a module to ground textual descriptions in anatomical evidence, allowing the model to maintain textual-visual consistency. By applying the two innovations, BoxMed-RL incorporates domain-specific clinical concepts and textual-visual alignment ability, effectively simulating the cognitive workflow of radiologists. BoxMed-RL integrates MCL, SVR and a downstream adapter in two sequential phases. The overall workflow of BoxMed-RL comprises the following: In the Pretraining Phase, our model is first fine-tuned via MCL using a structured radiological Chain-of-Thought (CoT) reasoning dataset to guide its learning of medical concepts; it then undergoes SVR, where reinforcement learning is applied to optimize spatial-textual alignment using Intersection-over-Union (IoU)-based rewards, ensuring that the generated phrases correspond to pixel-level anatomical evidence. In the Downstream Adapter Phase, BoxMed-RL’s weights are frozen and a lightweight adapter is fine-tuned on raw reports, producing fluent, clinically credible narratives while preserving the reasoning and spatial alignment learned earlier. The main contributions of our work are:

- We propose BoxMed-RL, a two-phase automated medical report generation model. To the best of our knowledge, BoxMed-RL is the first method to combine CoT reasoning and spatial grounding in medical report generation task.
- We introduce medical concept learning to force models to internalize the diagnostic logic of radiologists through hierarchical reasoning steps (e.g., Medical Findings → Disease Category → Anatomical Region), bridging the gap between free-form generation and clinically structured workflows.
- We introduce spatially verifiable reinforcement to explicitly align textual descriptions with anatomical regions (e.g., medical findings → bounding boxes) using IoU-based rewards.
- Extensive experiments on 2 public datasets demonstrate that BoxMed-RL achieves an average 7% improvement in natural language generation metrics compared to state-of-the-art methods. An average 5% improvement in large language model-based metrics further underscores BoxMed-RL’s robustness in generating high-quality radiology reports.

## 2. Related Work

### 2.1. Automated Medical Report Generation

With the advancements of deep learning in computer vision and natural language processing, many methods based on an encoder-decoder paradigm were proposed for automated generation of medical reports (Zhang et al., 2024c; Yang et al., 2022; Zhang et al., 2024b; Liu et al., 2021a;b; Miura et al., 2021). For the encoder component, these approaches differ in their input modalities, which include images, medical knowledge graphs, and extracted textual features. Several methods rely solely on X-ray images for report generation (Liu et al., 2021b; Miura et al., 2021). The first method (Liu et al., 2021b) leverages differences between diseased and normal X-ray images, while another method (Miura et al., 2021) enhances the language loss function by incorporating more fine-grained word-level features. Other major approaches would incorporate cross-modal features, integrating text, images, and graphs, to deliver additional expert insights, thereby enhancing and directing the entire report generation process (Zhang et al., 2024c; Yang et al., 2022; Zhang et al., 2024b; Liu et al., 2021a). In particular, rather than relying on manually designed graphs and injecting expert knowledge directly, certain methods enable models to autonomously learn the expert knowledge graph through node or edge prediction, thereby strengthening the model’s learning process (Zhang et al., 2024c;b).

### 2.2. Large Vision-Language Models in Medical Report Generation

Pretrained large language models, such as LLaMA (Touvron et al., 2023), GPT-4 (Achiam et al., 2023) have achieved remarkable success across a wide range of natural language processing tasks. However, due to the limited capability of large language models in handling cross-modal tasks, large vision-language models have been further developed to address multi-modality challenges by integrating both image and text inputs (Liu et al., 2024a; Wang et al., 2024; Chen et al., 2024). Emerging research refines the ap-

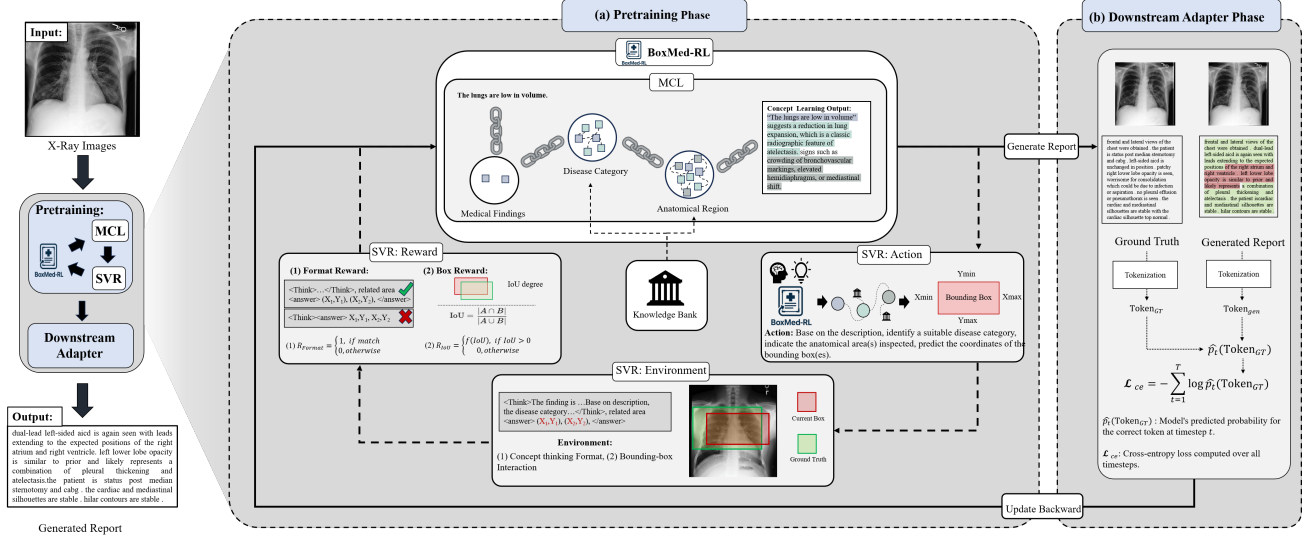


Figure 3. Overview of our BoxMed-RL framework, including 2 phases: (a) Pretraining Phase: The model first goes through MCL, enabling it to reason through structured medical concepts, mimicking radiologists’ diagnostic logic. Then it applies SVR, optimizing via reinforcement learning to align its concept reasoning with spatial regions in the image. (b) Downstream Adapter Phase: The model’s weight is frozen and a downstream task adapter is refined to help the model generate fluent reports.

plication of large vision-language models within the medical domain, tailoring them to diverse downstream tasks such as medical report generation, visual question-answering, and the proposal of treatment options based on provided modalities (Li et al., 2023; Pan et al., 2025). In contrast to the conventional encoder-decoder framework, which often requires task-specific customization of architecture and training methodologies, large vision-language models offer a more versatile approach. Pretrained or fine-tuned on extensive datasets comprising medical image-text pairs, large vision-language models demonstrate the capability to address a diverse range of tasks, including medical visual question answering, cross-modal report generation, and bounding box prediction, with greater adaptability and efficiency (Pan et al., 2025; Achiam et al., 2023; Wang et al., 2024).

### 2.3. Reinforcement Learning in Large Vision-Language Models

After the pretraining phase of large vision-language models, fine-tuning is essential to achieve optimal performance in a specific domain (Zhang et al., 2024a;e). While large vision-language models offer remarkable flexibility across various input modalities, their performance may not match that of deep learning models tailored to particular tasks. However, leveraging their pretrained knowledge and applying sufficient downstream fine-tuning, large vision-language models have the potential to outperform traditional deep learning models. Supervised fine-tuning and reinforcement fine-tuning are two primary approaches to adopt a model to

a specific task or domain. Supervised fine-tuning leverages paired data, such as in language translation tasks (Zhang et al., 2024a;e). For instance, we prompt the model to learn direct sentence translations and utilize token-wise classification loss to assess performance and update the model parameters. Instead of relying on a supervised loss function to steer the model’s learning, reinforcement fine-tuning leverages a reward signal, typically derived from human preferences to guide the model development (Ouyang et al., 2022; Chu et al., 2025). In the context of medical report generation, we utilize paired medical images and corresponding reports via supervised fine-tuning to enhance the model’s capability to generate accurate reports. However, this method lacks explainability, as it does not elucidate the reasoning behind the focus areas of the large vision-language models or the basis for their generated responses (Chu et al., 2025). To address this limitation, reinforcement learning from verifiable rewards, a technique within the broader framework of reinforcement fine-tuning, can be employed. Reinforcement fine-tuning enables the training of models to articulate their reasoning and justify their actions, thus improving explainability (Guo et al., 2025). Specifically, reinforcement learning from verifiable rewards leverages a reward model defined by a verification function, supplementing supervised loss with feedback delivered through reinforcement learning algorithms such as proximal policy optimization or group relative policy optimization. This approach refines the model’s decision-making process and enhances its explainability (Guo et al., 2025; Liu et al., 2025).



### 3. METHOD

#### 3.1. Overview

We propose BoxMed-RL, a two-phase training framework designed to enhance the explainability and clinical reliability of automated radiology report generation, leveraging the Qwen2-VL-2B (Wang et al., 2024) architecture. As illustrated in Fig. 3, our method sequentially integrates two main phases: **Pretraining Phase**: Initially, BoxMed-RL is fine-tuned via the medical concept learning module. We construct a structured dataset by decomposing radiology reports into explicit hierarchical reasoning steps (*Medical Findings*  $\rightarrow$  *Disease Category*  $\rightarrow$  *Anatomical Region*). This structured CoT dataset is used to guide the model’s training via supervised fine-tuning, enabling the model to internalize and replicate radiologists’ structured diagnostic logic. Next, BoxMed-RL goes through the spatially verifiable reinforcement module, which applies reinforcement learning to optimize textual-visual alignment between medical descriptions and anatomical regions. This process employs IoU-based rewards, explicitly grounding diagnostic phrases within precise anatomical regions via predicted bounding boxes, thereby ensuring verifiable and accurate anatomical correlations. **Downstream Adapter Phase**: BoxMed-RL’s weights from previous phase are frozen, and an adapter is fine-tuned to refine the linguistic fluency of the generated reports while preserving learned textual-visual associations, thus ensuring outputs remain clinically fluent and anatomically accurate.

In the BoxMed-RL framework, at Pretraining Phase (Section 3.2), the medical concept learning (Section 3.2.1) and spatially verifiable reinforcement (Section 3.2.2) are introduced to enhance its explainability through hierarchical reasoning and anatomical grounding, while Downstream Adapter Phase (Section 3.3) serves as the final step to ensure the generation of fluent and coherent report.

#### 3.2. Pretraining Phase

In the Pretraining Phase, BoxMed-RL is fine-tuned through medical concept learning and spatially verifiable reinforcement to instill structured diagnostic reasoning and precise spatial grounding. These two modules equip BoxMed-RL with clinical knowledge and textual-visual grounding, serving as a foundation for Downstream Adapter Phase.

##### 3.2.1. MEDICAL CONCEPT LEARNING FOR RADIOLOGIST-LIKE STRUCTURED REASONING

The primary goal of medical concept learning (MCL) module is to allow the model to internalize the hierarchical diagnostic logic of radiologists, enabling transparent clinical reasoning. Inspired by the Chain-of-Thought prompting paradigm (Wei et al., 2022), we construct a struc-

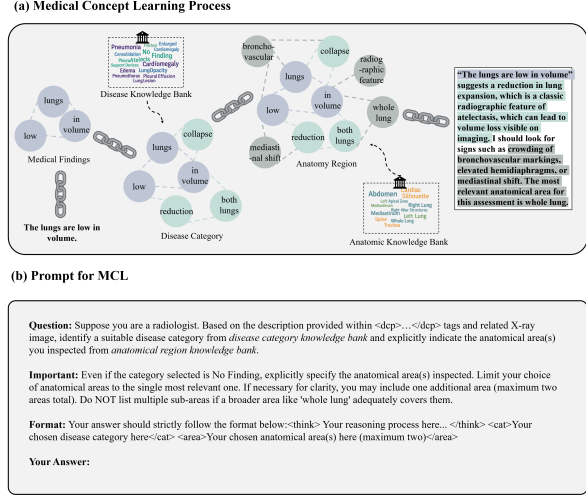


Figure 4. Implement details of MCL module. (a) Illustration of our medical concept learning via CoT formulation. (b) presents the prompt template used to guide the model’s reasoning.

tured radiological reasoning dataset that decomposes medical reports into hierarchical reasoning steps. Unlike conventional supervised fine-tuning that optimizes for report fluency, our approach explicitly structures training data into three domain-specific conceptual levels: (*Findings*  $\rightarrow$  *Disease Category*  $\rightarrow$  *Anatomical Region*) This mimics how radiologists progressively link observations (e.g., “ill-defined opacity”) to diagnoses (e.g., pneumonia) thus anchoring them to anatomy area (e.g., right middle lobe).

Two external medical information are integrated into the training paradigm. The Disease Category Knowledge Bank includes 14 clinical labels such as *pneumonia*, *fracture*, *consolidation*, *enlarged cardiomegaly*, *no finding*, *pleural other*, *cardiomegaly*, *pneumothorax*, *atelectasis*, *support devices*, *edema*, *pleural effusion*, *lung lesion*, and *lung opacity*, derived from CheXpert (Irvin et al., 2019). The Anatomical Region Knowledge Bank comprises 12 areas including *abdomen*, *cardiac silhouette*, *left apical zone*, *left hilar structures*, *left lung*, *mediastinum*, *right apical zone*, *right hilar structures*, *right lung*, *whole lung*, *spine*, and *trachea*, based on prior work (Yang et al., 2025).

During training, we first decompose raw reports into hierarchical reasoning chains (Fig. 4 (a)) using expert-curated mappings. For example: *Findings* (“Lungs are low in volume”)  $\rightarrow$  *Disease* (Atelectasis, via intermediate concepts like collapse and mediastinal shift)  $\rightarrow$  *Anatomy* (Whole Lung). Then using structured prompts (Fig. 4 (b)), we optimize the model to generate structured hierarchical CoT sequences. For a given training example consisting of a radiological image  $I$  and structured CoT annotations  $C$ , the BoxMed-RL  $\pi$ ’s parameters  $\theta$  are optimized to  $\theta'$  using a

Table 1. Comparison of different methods across various evaluation metrics in MIMIC-CXR. The best results are highlighted in **bold**. <sup>†</sup> indicates the result was reproduced.

Method	Year	BLEU-1	BLEU-2	BLEU-3	BLEU-4	METEOR	ROUGE-L	GEMA-Score	CheXpert	GreenScore
<b>Traditional Encoder-Decoder</b>										
R2Gen (Chen et al., 2020) <sup>†</sup>	2020	0.368	0.220	0.145	0.103	0.149	0.272	0.534	0.331	0.276
GSK (Yang et al., 2022)	2022	0.363	0.228	0.156	0.115	—	0.284	—	—	—
RECAP (Hou et al., 2023)	2023	<b>0.429</b>	0.267	0.177	0.125	0.168	0.288	—	—	—
<b>Region-Enhanced Encoder-Decoder</b>										
CMN (Chen et al., 2021) <sup>†</sup>	2021	0.353	0.213	0.140	0.098	0.162	0.279	0.530	0.342	0.295
CMM (Qin & Song, 2022)	2022	0.381	0.232	0.155	0.109	0.151	0.287	—	—	—
Clinical-BERT (Yan & Pei, 2022)	2022	0.383	0.230	0.151	0.106	0.144	0.275	—	—	—
MA (Wang et al., 2022a)	2022	0.396	0.244	0.162	0.115	0.151	0.274	—	—	—
METTransformer (Wang et al., 2023b)	2023	0.386	0.250	0.169	0.124	0.152	0.291	—	—	—
FMVP (Liu et al., 2024b)	2024	0.389	0.236	0.156	0.108	0.150	0.284	—	—	—
PromptMRG (Jin et al., 2024)	2024	0.398	—	—	0.112	0.157	0.268	—	<b>0.439</b>	—
RAMT (Zhang et al., 2024b)	2024	0.362	0.229	0.157	0.113	0.153	0.284	—	—	—
<b>Prompts-Driven Large Language Models</b>										
RGRG (Tanida et al., 2023) <sup>†</sup>	2023	0.300	0.182	0.120	0.082	0.156	0.249	0.553	0.360	0.246
R2GenGPT (Wang et al., 2023a)	2023	0.409	0.261	0.179	0.128	0.160	0.287	—	0.381	—
STREAM (Yang et al., 2025)	2025	0.420	0.267	0.184	0.133	0.164	0.291	—	0.392	—
<b>BoxMed-RL</b>										
Our BoxMed-RL	2025	0.426	<b>0.271</b>	<b>0.185</b>	<b>0.134</b>	<b>0.180</b>	<b>0.314</b>	<b>0.560</b>	0.412	<b>0.310</b>

cross-entropy loss:

$$\begin{aligned}\theta' &= \arg \min_{\theta} \mathcal{L}_{\text{MCL}}(\theta) \\ &= \arg \min_{\theta} - \sum_{t=1}^T \log p_{\theta}(c_t | I_t, c_{<t}),\end{aligned}\quad (1)$$

where  $\theta'$  is the optimized set of model parameters after training with the MCL objective,  $c_t$  denotes the  $t^{\text{th}}$  token of the structured CoT annotation, and  $c_{<t}$  represents preceding tokens.

By explicitly training the model to follow structured diagnostic reasoning chains, BoxMed-RL learns to produce clinically interpretable reports that mimic the radiologist’s analytical workflow, improving report explainability.

### 3.2.2. SPATIALLY VERIFIABLE REINFORCEMENT FOR ANATOMY LOCATION PERCEPTION

**Reinforcement Problem Statement:** While MCL module enables the model to mimic the flow of diagnostic reasoning, it lacks mechanisms to ensure spatial grounding of related textual descriptions, to bridge the gap between textual descriptions and anatomical evidence, we introduce the spatially verifiable reinforcement module (SVR). Building on the MCL module, SVR employs reinforcement learning with verifiable rewards through a group relative policy optimization framework to optimize two critical objectives: (1) Spatial consistency, ensuring that medical findings are aligned correctly with related anatomy regions. (2) Structured formatting, enforce the reasoning process before output the coordinate answer.

The overall process can be summarized as follows. In reinforcement learning with verifiable rewards, given a query  $q$ ,

the policy model BoxMed-RL  $\pi_{\theta'}$  (optimized after MCL) generates a response  $y$ , and receives the reward  $R(q, y)$ . The reinforcement learning with verifiable rewards objective encourages high-reward generations while regularizing the policy via KL divergence against a reference model  $\pi_{\text{ref}}$  (the frozen BoxMed-RL  $\pi_{\theta'}$ ):

$$\begin{aligned}\theta'' &= \arg \max_{\theta'} \mathbb{E}_{\text{SVR}}(\theta') \\ &= \arg \max_{\theta'} \mathbb{E}_{y \sim \pi_{\theta'}(q)} [R(q, y) - \beta \cdot \text{KL}(\pi_{\theta'}(y|q) \parallel \pi_{\text{ref}}(y|q))],\end{aligned}\quad (2)$$

where  $\theta''$  is the optimized set of model parameters after the SVR module and  $\beta$  is the hyperparameter to control KL divergence.

To improve sample efficiency and eliminate the need for a separate value estimator, we incorporate the group relative policy optimization algorithm (Guo et al., 2025). The algorithm operates by generating a group of responses for each query  $q$ :

$$\{y_1, \dots, y_N\} \sim \pi_{\theta'}(y | q), \quad (3)$$

where  $N$  is the number of groups.

For each response  $y_i$ , compute the total verifiable reward  $r_i$ , then compute the corresponding group relative policy optimization normalized score  $a_i$ :

$$a_i = \frac{r_i - \text{mean}(\{r_1, \dots, r_N\})}{\text{std}(\{r_1, \dots, r_N\})}. \quad (4)$$

We then substitute these scores into the reinforcement learning with verifiable rewards framework in Eq. (2), resulting

Table 2. Comparison of different methods across various evaluation metrics in IU X-Ray, grouped by method type. The best results are highlighted in **bold**.

Method	Year	BLEU-1	BLEU-2	BLEU-3	BLEU-4	METEOR	ROUGE-L	CheXpert
<b>Traditional Encoder-Decoder</b>								
R2Gen (Chen et al., 2020)	2020	0.475	0.304	0.219	0.170	0.187	0.371	0.530
GSK (Yang et al., 2022)	2022	0.496	0.327	0.238	0.178	—	0.381	—
<b>Region-Enhanced Encoder-Decoder</b>								
CMN (Chen et al., 2021)	2021	0.475	0.309	0.222	0.170	0.191	0.375	0.552
CMM (Qin & Song, 2022)	2022	0.494	0.321	0.235	0.181	0.201	0.384	—
Clinical-BERT (Yan & Pei, 2022)	2022	0.495	0.330	0.231	0.170	0.209	0.376	—
MA (Wang et al., 2022a)	2022	<b>0.500</b>	0.328	0.230	0.170	0.213	0.386	—
METransformer (Wang et al., 2023b)	2023	0.483	0.332	0.228	0.172	0.192	0.380	—
FMVP (Liu et al., 2024b)	2024	0.485	0.315	0.225	0.169	0.201	0.398	—
PromptMRG (Jin et al., 2024)	2024	0.401	—	—	0.098	0.160	0.281	0.556
RAMT (Zhang et al., 2024b)	2024	0.482	0.310	0.221	0.165	0.195	0.377	—
<b>Prompts-Driven Large Language Models</b>								
R2GenGPT (Wang et al., 2023a)	2023	0.491	0.323	0.234	0.180	0.211	0.376	0.601
STREAM (Yang et al., 2025)	2025	0.499	<b>0.333</b>	0.238	<b>0.178</b>	0.213	0.377	0.608
<b>BoxMed-RL</b>								
Our BoxMed-RL	2025	0.490	0.320	<b>0.240</b>	<b>0.178</b>	<b>0.220</b>	<b>0.404</b>	<b>0.610</b>

Table 3. Classification metrics across 14 categories of CheXpert.

Category	Accuracy	Precision	Recall	F1-Score
No Finding	0.892	0.651	0.739	0.681
Cardiomediastinum	0.594	0.389	0.386	0.386
Cardiomegaly	0.581	0.418	0.419	0.418
Lung Lesion	0.899	0.361	0.341	0.338
Lung Opacity	0.579	0.397	0.393	0.388
Edema	0.689	0.429	0.422	0.425
Consolidation	0.838	0.380	0.363	0.368
Pneumonia	0.756	0.383	0.369	0.373
Atelectasis	0.623	0.418	0.424	0.420
Pneumothorax	0.927	0.372	0.378	0.375
Pleural Effusion	0.648	0.457	0.457	0.456
Pleural Other	0.937	0.319	0.326	0.323
Fracture	0.911	0.335	0.334	0.331
Support Devices	0.739	0.485	0.492	0.488

in the following hybrid optimization objective:

$$\theta'' = \arg \max_{\pi_{\theta''}} \mathbb{E}_{y_i \sim \pi_{\theta''}(q)} [a_i - \beta \cdot \text{KL}(\pi_{\theta''}(y_i|q) \parallel \pi_{\text{ref}}(y_i|q))], \quad (5)$$

where  $a_i$  reflects the relative advantage of response  $y_i$  within the group. This hybrid strategy allows BoxMed-RL to explicit supervision of verifiable reward signals with the efficiency and stability of relative policy optimization.

**IoU Reward for Spatially Alignment:** To promote anatomically precise and spatially verifiable ability, we incorporate an IoU-based reward as a core component of our reinforcement learning strategy. This reward function explicitly guides the model to align diagnostic descriptions with correct image regions, reinforcing textual-visual grounding during policy optimization.

Each predicted bounding box is represented by its corner coordinates  $(x_1, y_1)$  and  $(x_2, y_2)$ , where  $(x_1, y_1)$  defines the top-left corner and  $(x_2, y_2)$  defines the bottom-right corner of the bounding area. The IoU between a predicted box  $B_{\text{pred}}$  and a ground truth bounding box  $B_{\text{gt}}$  is computed as:

$$\text{IoU}(B_{\text{pred}}, B_{\text{gt}}) = \frac{|B_{\text{pred}} \cap B_{\text{gt}}|}{|B_{\text{pred}} \cup B_{\text{gt}}|}, \quad (6)$$

where  $\text{IoU} \in [0, 1]$ .

This metric quantifies the degree of overlap between the predicted and actual regions. A high IoU score indicates strong spatial alignment, while a low score penalizes incorrect or irrelevant location. We then define the spatial reward as:

$$\mathcal{R}_{\text{IoU}} = \begin{cases} \text{IoU}, & \text{if } \text{IoU} > 0 \\ 0, & \text{otherwise} \end{cases}. \quad (7)$$

This reward is integrated into our total verifiable reward  $R$ , alongside a format reward  $\mathcal{R}_{\text{format}}$  that ensures structural correctness of the generated output.

By leveraging IoU as a direct spatial alignment metric, our approach encourages BoxMed-RL to remain textual-visual consistency.

**Format Reward for Structured Output:** To complement spatial alignment, we enforce the output format using a binary reward signal  $\mathcal{R}_{\text{format}}$ :

$$\mathcal{R}_{\text{format}} = \begin{cases} 1, & \text{if } t_y \in t \\ 0, & \text{otherwise} \end{cases}, \quad (8)$$

Table 4. Ablation study results to include or exclude different components of BoxMed-RL. A one-tailed Wilcoxon signed-rank test is performed on each ablated model, with \* indicating a p-value less than 0.05 and \*\* indicating a p-value less than 0.01.

Configuration	MCL	SVR	Adapter	BLEU-1	BLEU-2	BLEU-3	BLEU-4	METEOR	ROUGE-L	GEMA-Score	CheXpert	GreenScore
w/o MCL & SVR	✗	✗	✓	0.385**	0.235**	0.156**	0.110**	0.173**	0.285**	0.531**	0.393**	0.270**
w/o SVR	✓	✗	✓	0.393**	0.239**	0.159**	0.112**	0.173**	0.288**	0.540**	0.398**	0.280**
w/o MCL	✗	✓	✓	0.392**	0.241**	0.160**	0.112**	0.177**	0.290**	0.551**	0.406**	0.292**
BoxMed-RL	✓	✓	✓	0.426	0.271	0.185	0.134	0.180	0.314	0.560	0.412	0.310

where  $t_y$  is the response  $y$ 's format,  $t$  has the form of  $\langle \text{think} \rangle \dots \langle / \text{think} \rangle, \langle \text{answer} \rangle \dots \langle / \text{answer} \rangle$ . This format reward encourages the model to output its reasoning process and spatial answer in a structured format.

**Reward Combination and Objective Updated:** Given the query  $q$ , the total verifiable reward  $R$  for each response  $y_i$  is the additive combination of  $\mathcal{R}_{\text{IoU}}$  and  $\mathcal{R}_{\text{format}}$ :

$$R(q, y_i) = \mathcal{R}_{\text{IoU}}(q, y_i) + \mathcal{R}_{\text{format}}(q, y_i). \quad (9)$$

We then use Eq. (9) to substitute  $r_i$  in Eq. (4), thus Eq. (4) is updated as:

$$A(q, y_i) = \frac{R(q, y_i) - \text{mean}(\{R(q, y_j)\}_{j=1}^N)}{\text{std}(\{R(q, y_j)\}_{j=1}^N)}. \quad (10)$$

Therefore, our hybrid optimization objective in Eq. (5) can be updated as:

$$\theta'' = \arg \max_{\pi_{\theta''}} \mathbb{E}_{y_i \sim \pi_{\theta''}(q)} [A(q, y_i) - \beta \cdot \text{KL}(\pi_{\theta''}(y_i|q) \parallel \pi_{\text{ref}}(y_i|q))]. \quad (11)$$

This formulation jointly optimizes for verifiable structure and anatomical alignment, allowing BoxMed-RL to correctly relate descriptions with spatial information.

### 3.3. Downstream Adapter Phase

Following Pretraining, we freeze the BoxMed-RL backbone and attach a lightweight LoRA (Hu et al., 2022) adapter  $\pi_{\text{Adapter}}$  to refine the fluency and clinical fidelity of the generated reports. While Pretraining emphasizes structured diagnostic reasoning and spatial grounding, the purpose of this adapter is not to overwrite these learned capabilities but rather to enhance the surface-level linguistic quality by aligning the outputs to the distribution of professional radiology reports.

Specifically, we train *Adapter*, initialized from the pretrained parameters  $\theta''$ , using a large corpus of chest X-ray images  $\{I_1, \dots, I_M\}$  paired with corresponding radiology reports  $\{o_1, \dots, o_M\}$ . The *Adapter*'s parameters  $\hat{\theta}$  are op-

timized using a cross-entropy loss:

$$\begin{aligned} \hat{\theta} &= \arg \min_{\theta''} \mathcal{L}_{\text{Adapter}}(\theta'') \\ &= \arg \min_{\theta''} - \sum_{m=1}^M \log p_{\theta''}(y_m | I_m, y_{<m}), \end{aligned} \quad (12)$$

where  $p_{\theta''}(y_m | I_m, y_{<m})$  denotes the probability of generating token  $y_m$  given the input image  $I_m$  and previously generated tokens  $y_{<m}$ . By updating only the adapter's weights, the pretrained reasoning and spatial-grounding skills remain preserved, enabling *Adapter* to effectively learn expert clinical phrasing and linguistic fluency suitable for healthcare workflows. The learning process of our BoxMed-RL can be summarized as Algorithm 1 shown in Appendix.

## 4. Experiments and Analysis

### 4.1. Datasets and Evaluation Metrics

In the Pretraining Phase of BoxMed-RL, we employ two bounding box-sentence pair datasets: MS-CXR (Boecking et al., 2022) and LATTE-CXR (Ghelichkhan & Tasdizen, 2025). MS-CXR, sourced from MIMIC-CXR (Johnson et al., 2019), includes 1,162 image-sentence pairs with annotated bounding boxes and corresponding medical phrases. LATTE-CXR, built from MIMIC-CXR and REFLACX (Bigolin Lanfredi et al., 2022), offers 13,751 verified bounding box annotations aligned with radiological findings. Both datasets label samples with medical findings and their spatial regions. In the Downstream Adapter Phase, we train the *Adapter* using two radiology report generation benchmarks: MIMIC-CXR and IU X-Ray (Demner-Fushman et al., 2016). MIMIC-CXR comprises 377,110 chest X-ray images paired with 227,835 radiology reports, while IU X-Ray includes 7,470 images and 3,955 reports. For both, we target the "findings" section of each report for generation.

We evaluate BoxMed-RL using three metric categories to assess its clinical trustworthiness and technical performance. First, to evaluate fluency, coherence, and lexical similarity, we employ standard natural language generation (NLG) metrics: BLEU (Papineni et al., 2002), ROUGE (Recall-oriented) (Lin, 2004), and METEOR (Lavie & Agarwal, 2007). Second, we measure clinical efficacy (CE) by evaluating how well the generated reports capture medically relevant concepts by using CheXpert (Irvin et al., 2019). This is



quantified using standard classification metrics including F1 score, precision, and recall. Third, we adopt advanced large language model based metrics, GEMA-Score (Zhang et al., 2025) and GreenScore (Ostmeier et al., 2024), to assess clinical accuracy and reliability.

## 4.2. Implementation Details

Several preprocessing strategies and training configurations are adopted to optimize our BoxMed-RL performance, based on the Qwen2-VL-2B architecture. All chest X-ray images are resized to one-quarter of their original height and width to preserve aspect ratio while reducing memory consumption. Correspondingly, all bounding box coordinates are resized using the same ratio to maintain consistency in spatial supervision. For text targets, we extract the ‘findings’ section from each radiology report, removing excess whitespace, special characters, and entries with empty or missing findings.

In the Pretraining Phase, we train the MCL module using the AdamW optimizer with an initial learning rate of  $1e-4$ , applying a cosine learning rate schedule for 2 epochs. For the SVR module, we adopt the architecture and hyperparameter settings from Visual-RFT (Liu et al., 2025), training for 4 epochs. In the Downstream Adapter Phase, we freeze the BoxMed-RL backbone and train a lightweight LoRA adapter, configured with rank  $r = 8$  for 2 epochs. All experiments are conducted with a batch size of 1 on NVIDIA H100 GPUs.

## 4.3. Quantitative Results

We conduct a comprehensive comparative study of various frameworks, including **traditional encoder-decoder models**: R2Gen (Chen et al., 2020), GSK (Yang et al., 2022), RECAP (Hou et al., 2023); **region-enhanced encoder-decoder models**: MA (Wang et al., 2022a), CMN (Chen et al., 2021), CMM (Qin & Song, 2022), Clinical-Bert (Yan & Pei, 2022), METransformer (Wang et al., 2023b), PromptMRG (Jin et al., 2024), FMVP (Liu et al., 2024b); and **prompt-driven large language models**: STREAM (Yang et al., 2025), R2GenGPT (Wang et al., 2023a) and RGRG (Tanida et al., 2023). Under the defined frameworks, the deep learning models employ distinct architectures for visual feature extraction and decoding. ResNet serves as the visual encoder in R2Gen, CMN, CMM, GSK, and PromptMRG. In contrast, DenseNet is utilized by Clinical-BERT, RAMT, FMVP, and MA to capture dense visual representations. RGRG adopts Faster R-CNN for region-specific feature extraction through bounding box detection. Meanwhile, Vision Transformers are employed by METransformer, R2GenGPT, RECAP, and STREAM, harnessing self-attention mechanisms to model global image context. For decoding, RGRG, R2GenGPT, and STREAM integrate large language models to gener-

ate coherent reports, capitalizing on their advanced generative abilities. Conversely, the remaining frameworks utilize transformer-based architectures or their variants as decoders, enabling effective sequential text generation. BoxMed-RL differs from other models by employing a large vision-language model that merges visual and textual encoder functions into a single unified model.

### 4.3.1. NATURAL LANGUAGE GENERATION METRICS

BoxMed-RL demonstrates significant performance in NLG metrics, achieving state-of-the-art performance in BLEU-3 and BLEU-4 scores across two datasets: MIMIC-CXR (0.185 and 0.134, Table 1) and IU X-ray (0.240 and 0.178, Table 2), with an average improvement 7% in both METEOR and ROUGE-L metric. These findings underscore BoxMed-RL’s consistent performance, even on external datasets not included in the Pretraining Phase. Associating observations with relevant concepts enables models to generate contextually accurate sentences with appropriate terminology, improving BLEU-3 and BLEU-4 scores while maintaining BLEU-1 and BLEU-2 performance comparable to state-of-the-art models.

### 4.3.2. CLINICAL EFFICACY METRICS

BoxMed-RL also demonstrates stable performance in analyzing clinical concepts, achieving CE metrics with F1 score of 0.412 on MIMIC-CXR and 0.610 on IU X-ray. This consistency contrasts with PromptMRG, which exhibits unstable performance, ranking highest in MIMIC-CXR but fourth in IU X-ray. As presented in Table 3, BoxMed-RL achieves high accuracy in detecting the “No Finding” and “Support Devices” categories. Additionally, the model demonstrates stable performance across disease classifications, with F1 scores ranging from a maximum of 0.456 to a minimum of 0.323. This narrow range indicates consistent performance with low variance, suggesting that the model avoids erratic predictions and maintains reliability across different disease classes. Leveraging advanced large language model based metrics, such as readability, coherence, and report completeness, BoxMed-RL also achieves outstanding performance, with a 5% enhancement in each metric, further underscoring its robustness in generating high-quality radiology reports. Overall, BoxMed-RL demonstrates excellent and stable performance among three metric categories across two datasets.

## 4.4. Ablation Studies

### 4.4.1. IMPACTS OF THE COMPONENTS IN BOXMED-RL

In this section, we conduct comprehensive ablation studies to evaluate the contribution of each component within our BoxMed-RL framework. Three experiments were designed, each excluding key components of the model to assess their

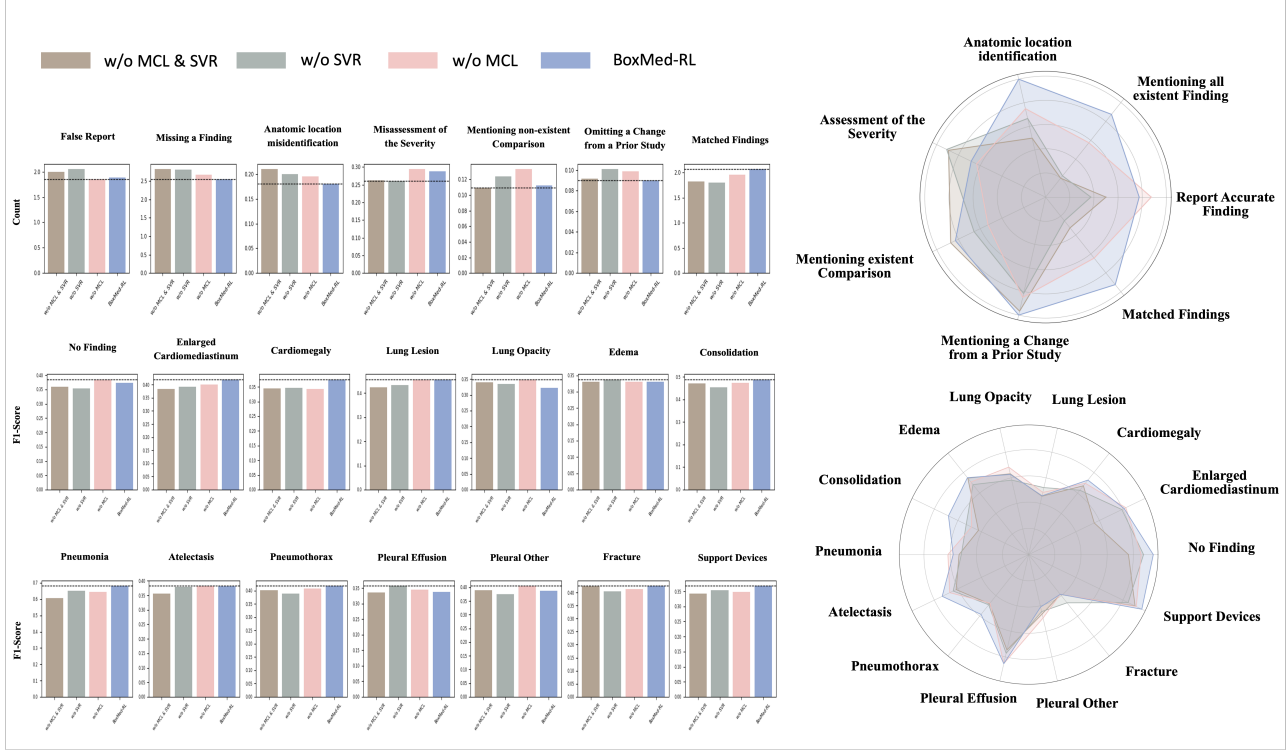


Figure 5. Comprehensive analysis of each ablation module’s performance on Green score 7 clinical evaluation criteria and CheXpert 14 categories classification. Bar charts display the detailed values for each category, while the radar chart on the right illustrates the overall performance of each ablated model. In the bar charts, the black line indicates the best performance in each category.

impact on overall performance. A one-tailed Wilcoxon signed-rank test is conducted on each experiment’s results to determine if Group 1’s values are significantly lower than Group 2’s. The results, presented in Table 4, demonstrates that the final framework, BoxMed-RL, leads to the best performance. With adapter alone, no extra knowledge is acquired through MCL or SVR. Consequently, the large vision-language model solely develops the capacity to generate reports from X-ray images, focusing on report generation proficiency. However, it lacks the ability to reasoning and make observations. For example, while it may detect an abnormality in an X-ray image, it might not identify the specific region or provide additional cues that could aid in further diagnostic analysis. Conversely, incorporating either MCL or SVR improves performance in NLG metrics, with average gains of 3% (for SVR) and 7% (for MCL) in BLEU scores, and disease classification metrics. These improvements stem from the integration of radiologist domain expertise and visual cues from the image. For instance, in MCL, employing a radiologist’s chain of reasoning, such as associating a detected abnormality with related pathologies, enhances the model’s ability to generate accurate and contextually relevant reports. Without MCL, the model’s performance is comparable to that without SVR

but remains slightly lower ( 3% ) in disease classification metrics. This is because having the ability observe X-ray images better assist in identifying abnormalities. Although SVR aligns sentences with image features, enabling large vision-language models to better identify regions requiring attention and generate corresponding reports, it does not provide the reasoning capabilities derived from MCL. By integrating all components, BoxMed-RL demonstrates superior X-ray report generation capabilities, as evidenced by an average 22% improvement in the BLEU score and a 10% increase in the CE metric. Its reasoning and visual alignment capabilities enable the model to effectively leverage text-image relationships.

As detailed in Fig. 5, BoxMed-RL demonstrates significant performance improvements compared to other ablated models. From the perspective of the GreenScore, we evaluated each model on seven clinical evaluation criteria: False report of a finding in the candidate, Missing a finding present in the reference, Misidentification of a finding’s anatomic location/position, Misassessment of the severity of a finding, Mentioning a comparison that is not in the reference, Omitting a comparison detailing a change from a prior study, and the number of matched findings (Ostmeier et al., 2024).

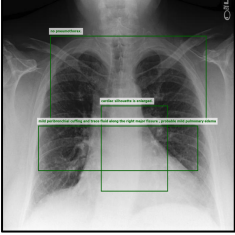
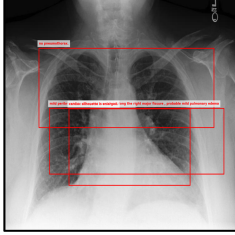
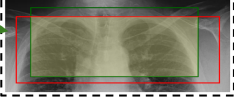

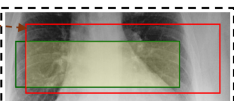
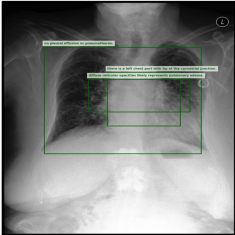
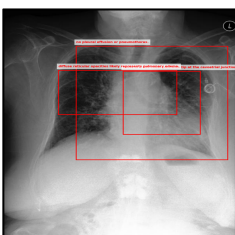

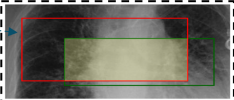
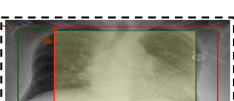
 <p>Ground Truth</p>  <p>Prediction</p>	<p><b>Ground Truth Report:</b></p> <p>lung volumes within normal limits. <b>cardiac silhouette is enlarged. mild peribronchial cuffing and trace fluid along the right major fissure, probable mild pulmonary edema. no pneumothorax. no acute osseous abnormality.</b></p> <p><b>Predicted Report:</b></p> <p><b>the lungs are clear without, pneumothorax. there is mild cardiomegaly. subtle fluid along the right major fissure, probable mild pulmonary edema. no acute osseous abnormalities identified.</b></p>	<p><b>the lungs are clear without, pneumothorax</b></p> <p>&lt;think&gt; The description suggests that the examination was focused on ruling out <b>the presence of air in the pleural space</b>. Since no pneumothorax was found, the appropriate category would be <b>"No Findings."</b> The most relevant anatomical area inspected for pneumothorax would be <b>the "whole lung,"</b> as this condition involves the lung fields. &lt;/think&gt;</p> <p><b>there is mild cardiomegaly</b></p> <p>&lt;think&gt; The description suggests an issue related to <b>the heart size</b>. The most relevant disease category for an enlarged cardiac silhouette is <b>"Cardiomegaly."</b> The anatomical area inspected is the <b>"cardiac silhouette"</b> as it directly pertains to the <b>heart's size and shape</b>. &lt;/think&gt;</p> <p><b>subtle fluid along the right major fissure</b></p> <p>&lt;think&gt; The description suggests that there are indicative of fluid accumulation in the lungs. This <b>aligns with the presence of pulmonary edema</b>. The right major fissure is part of the right lung, so the most relevant anatomical area to inspect would be the <b>right lung</b>. &lt;/think&gt;</p>  <p>Prediction : (124,139,683,350) Ground Truth : (164, 110, 624, 330) <b>IOU : 0.6703</b></p>  <p>Prediction : (220, 300, 607, 504) Ground Truth : (314, 291, 510, 512) <b>IOU : 0.4860</b></p>  <p>Prediction : (158, 299, 715, 474) Ground Truth : (129, 343, 599, 459) <b>IOU : 0.5058</b></p>
 <p>Ground Truth</p>  <p>Prediction</p>	<p><b>Ground Truth Report:</b></p> <p>there is a <b>left chest port with tip at the cavoatrial junction. diffuse reticular opacities likely represents pulmonary edema. the heart is normal size. no pleural effusion or pneumothorax. no acute osseous abnormalities.</b></p> <p><b>Predicted Report:</b></p> <p><b>left-sided port-a-cath tip, heart size is norma. mediastinal and hilar contours are unchanged. there is mild-to-moderate pulmonary edema. no focal consolidation, pleural effusion or pneumothorax is identified.</b></p>	<p><b>left-sided port-a-cath tip</b></p> <p>&lt;think&gt; The description indicates <b>the presence of a support device</b>. This is not indicative of any disease but rather a medical intervention. The most relevant anatomical area to inspect for the placement of a chest port is the <b>mediastinum</b>.&lt;/think&gt;</p> <p><b>there is mild-to-moderate pulmonary edema</b></p> <p>&lt;think&gt; The description suggests the <b>presence of fluid accumulation in the lungs</b>, which is characteristic of <b>edema</b>. The anatomical area that would be inspected for such a finding is the <b>"whole lung"</b> as pulmonary edema affects the lung tissue diffusely. &lt;/think&gt;</p> <p><b>no focal consolidation, pleural effusion or pneumothorax is identified</b></p> <p>&lt;think&gt;The disease categories provided include Pleural Effusion and Pneumothorax, which are specific conditions related to the lungs. The most suitable category is <b>Pleural Effusion</b>, as it directly relates to the presence of fluid in the pleural space. The anatomical area inspected would be the <b>whole lung</b>, as it encompasses <b>the pleural space where effusions are typically assessed</b>.&lt;/think&gt;</p>  <p>Prediction : (315,222,512,420) Ground Truth : (278, 242, 474, 413) <b>IOU : 0.5998</b></p>  <p>Prediction : (150, 219, 452, 358) Ground Truth : (228, 264, 500, 368) <b>IOU : 0.4279</b></p>  <p>Prediction : (195,143,582,500) Ground Truth : (109, 161, 530, 502) <b>IOU : 0.6754</b></p>

Figure 6. Representative cases of our BoxMed-RL, selected because they include clinically subtle findings that are challenging for automated systems, showcasing the model’s potential to perform well on challenging findings. Each row shows a real patient case with visual and textual outputs. The first column presents the X-ray image with the ground-truth (green) and predicted (red) bounding boxes. The second column compares the ground-truth report with the report generated by BoxMed-RL. The third column shows BoxMed-RL’s reasoning process and detected regions.

For the first six criteria, the Green Score counts errors, so lower values indicate better performance; for the number of matched findings, higher values are better. The radar chart shows that BoxMed-RL achieves holistic performance across all seven areas, with an average improvement of 6% compared to other ablated models. Notably, for misidentification of anatomic location, BoxMed-RL and the model without MCL perform best, as they include the SVR module for visual alignment. The CheXpert 14 categories classification results are shown following the GreenScore (Irvin

et al., 2019). Among the 14 classes, BoxMed-RL demonstrates the best performance in eight classes, including Enlarged Cardiomediastinum, Cardiomegaly, Lung Lesion, Consolidation, Support Devices, Fracture, Pneumothorax, and Atelectasis, with an average percentage improvement of 5.11% compared to the model without MCL and SVR modules, 3.50% compared to the model without SVR, and 2.83% compared to the model without MCL. The results also demonstrate that either the SVR or MCL module can improve both clinical metrics and disease classification met-

Table 5. Comparison of different training strategies for the adaptation of the report generation task. A one-tailed Wilcoxon signed-rank test is performed on each strategy, with \* indicating a p-value less than 0.05 and \*\* indicating a p-value less than 0.01.

Vision Tower	Projector	Adapter	BLEU-1	BLEU-2	BLEU-3	BLEU-4	METEOR	ROUGE-L	CheXpert
✓	✗	✗	0.379**	0.230**	0.151**	0.105**	0.171**	0.282**	0.388**
✗	✓	✗	0.380**	0.234**	0.155**	0.109**	0.175**	0.287**	0.393**
✓	✗	✓	0.390**	0.237**	0.157**	0.110**	0.173**	0.288**	0.390**
✗	✓	✓	0.394**	0.242**	0.161**	0.114**	0.174**	0.288**	0.389**
✗	✗	✓	0.426	0.271	0.185	0.134	0.180	0.314	0.412

rics, highlighting their effectiveness.

#### 4.4.2. IMPACTS OF DIFFERENT TRAINING STRATEGIES

Within the BoxMed-RL framework, it primarily consists of a vision tower, a component of the large vision-language model where the image is encoded; a projector, which is used to project the encoded image features for the subsequent language model to process; and a language model to decode these inputs for meaningful text generation. In this section, we evaluated various training strategies for BoxMed-RL, including: (1) freezing either the vision tower or the projector, and (2) incorporating an adapter into the language model. From Table 5, the training strategies for adapting report generation tasks produce comparable CheXpert scores, demonstrating that the generated reports closely align with the clinical semantic content of ground truth reports. This consistency highlights the robustness of the Pre-training Phase. However, with the inclusion of an adapter, BoxMed-RL generates better-formatted reports, achieving higher scores on NLG metrics. Notably, the best results were achieved without training the vision tower or projector. This outcome likely stems from the pretraining phase, where the vision tower and projector already developed the ability to associate sentences with visual features. Fine-tuning them may lead to performance degradation.

#### 4.5. Case Studies

As depicted in Fig. 6, we present two detailed case studies evaluated using the BoxMed-RL model. These cases were chosen because they include clinically relevant and often subtle findings (e.g., mild cardiomegaly, pulmonary edema, support devices) that are commonly misclassified in prior work and remain challenging for automated systems. Despite these challenges, BoxMed-RL successfully identifies and localizes the conditions, demonstrating strong performance and explainability on real-world examples. For the first case, the attention area is broadly surrounding the lungs, while the second case contains more specific findings near the heart. The cases encompass both normal and abnormal findings, including the presence of supporting devices, to enable a comprehensive evaluation of the robustness of BoxMed-RL. The ground truth and the model’s

predicted reports are shown in the middle column, with semantically similar sentences highlighted in matching colors. This visual representation underscores the capability of BoxMed-RL to generate X-ray descriptions in a radiologist-like tone, achieving close alignment with the ground truth reports. In the right column, bounding boxes are provided, corresponding to selected sentences from the generated reports, which illustrate the model’s explainability. Given a predicted report, it is essential to demonstrate how BoxMed-RL constructs each sentence by articulating its reasoning and visual observations, identifying which image regions inform the sentence and justifying their relevance. For instance, consider the sentence “There is mild cardiomegaly”: the model observes that this statement pertains to the size of the heart, specifically indicating a condition of slight enlargement. Accordingly, the model may focus on the region near the heart, depicted with a red bounding box. BoxMed-RL, leveraging domain-specific knowledge learned from MCL, further associates the sentence “There is mild cardiomegaly” with the term “cardiac silhouette” a radiological term describing the heart’s outline in imaging studies, which is present in the ground truth report. By integrating these extended insights with bounding boxes, we gain a transparent understanding of the model’s focus areas and the rationale behind its attention to specific regions, enhancing both explainability and trustworthiness.

## 5. Conclusion

In this work, we present BoxMed-RL, a novel framework that advances chest X-ray report generation by unifying medical concept learning and spatially verifiable reinforcement. By decomposing reports into hierarchical reasoning steps (Findings → Disease → Anatomy) and enforcing textual-visual alignment via IoU rewards, BoxMed-RL addresses two critical challenges: (1) the mismatch between model outputs and radiologists’ structured diagnostic workflows, and (2) the misalignment between textual descriptions and visual evidence. Experiments on two benchmarks demonstrate that BoxMed-RL outperforms state-of-the-art methods across language quality, clinical accuracy, and composite metrics. Despite its strong performance, BoxMed-RL has limitations. Currently, it is tailored for chest X-ray analysis,



and its effectiveness on other imaging modalities, such as CT or MRI, remains unexplored. The reliance on bounding box annotations for spatial supervision may limit scalability, as such data is costly to acquire. In future work, we aim to extend BoxMed-RL to support multi-modal radiology tasks, adapt it to 3D volumetric data, and explore self-supervised or retrieval-augmented approaches for improving generalization. We also envision integrating user feedback or human-in-the-loop training to further enhance clinical applicability and safety.

## References

- Achiam, J., Adler, S., Agarwal, S., Ahmad, L., Akkaya, I., Aleman, F. L., Almeida, D., Altschmidt, J., Altman, S., Anadkat, S., et al. Gpt-4 technical report. *arXiv preprint arXiv:2303.08774*, 2023.
- Bigolin Lanfredi, R., Zhang, M., Auffermann, W. F., Chan, J., Duong, P.-A. T., Srikumar, V., Drew, T., Schroeder, J. D., and Tasdizen, T. Reflax, a dataset of reports and eye-tracking data for localization of abnormalities in chest x-rays. *Scientific data*, 9(1):350, 2022.
- Boecking, B., Usuyama, N., Bannur, S., Castro, D. C., Schwaighofer, A., Hyland, S., Wetscherek, M., Naumann, T., Nori, A., Alvarez-Valle, J., et al. Making the most of text semantics to improve biomedical vision-language processing. In *European conference on computer vision*, pp. 1–21. Springer, 2022.
- Brady, A., Laoide, R. Ó., McCarthy, P., and McDermott, R. Discrepancy and error in radiology: concepts, causes and consequences. *The Ulster medical journal*, 81(1):3, 2012.
- Chen, Z., Song, Y., Chang, T.-H., and Wan, X. Generating radiology reports via memory-driven transformer. *arXiv preprint arXiv:2010.16056*, 2020.
- Chen, Z., Shen, Y., Song, Y., and Wan, X. Cross-modal memory networks for radiology report generation. In *Proceedings of the 59th Annual Meeting of the Association for Computational Linguistics and the 11th International Joint Conference on Natural Language Processing (Volume 1: Long Papers)*, pp. 5904–5914, Online, August 2021. Association for Computational Linguistics.
- Chen, Z., Wu, J., Wang, W., Su, W., Chen, G., Xing, S., Zhong, M., Zhang, Q., Zhu, X., Lu, L., Li, B., Luo, P., Lu, T., Qiao, Y., and Dai, J. Internvl: Scaling up vision foundation models and aligning for generic visual-linguistic tasks. In *Proceedings of the IEEE/CVF Conference on Computer Vision and Pattern Recognition (CVPR)*, pp. 24185–24198, June 2024.
- Chu, T., Zhai, Y., Yang, J., Tong, S., Xie, S., Schuurmans, D., Le, Q. V., Levine, S., and Ma, Y. Sft memorizes, rl generalizes: A comparative study of foundation model post-training. *arXiv preprint arXiv:2501.17161*, 2025.
- Delrue, L., Gosselin, R., Ilsen, B., Van Landeghem, A., de Mey, J., and Duyck, P. Difficulties in the interpretation of chest radiography. *Comparative interpretation of CT and standard radiography of the chest*, pp. 27–49, 2011.
- Demner-Fushman, D., Kohli, M. D., Rosenman, M. B., Shooshan, S. E., Rodriguez, L., Antani, S., Thoma, G. R., and McDonald, C. J. Preparing a collection of radiology examinations for distribution and retrieval. *Journal of the American Medical Informatics Association*, 23(2): 304–310, 2016.
- Gao, D., Kong, M., Zhao, Y., Huang, J., Huang, Z., Kuang, K., Wu, F., and Zhu, Q. Simulating doctors’ thinking logic for chest x-ray report generation via transformer-based semantic query learning. *Medical Image Analysis*, 91:102982, 2024.
- Ghelichkhan, E. and Tasdizen, T. LATTE-CXR: Locally Aligned Text and image, Explainable Dataset for Chest X-Rays, version 1.0.0, 2025.
- Goergen, S. K., Pool, F. J., Turner, T. J., Grimm, J. E., Appleyard, M. N., Crock, C., Fahey, M. C., Fay, M. F., Ferris, N. J., Liew, S. M., et al. Evidence-based guideline for the written radiology report: Methods, recommendations and implementation challenges. *Journal of medical imaging and radiation oncology*, 57(1):1–7, 2013.
- Guo, D., Yang, D., Zhang, H., Song, J., Zhang, R., Xu, R., Zhu, Q., Ma, S., Wang, P., Bi, X., et al. Deepseek-r1: Incentivizing reasoning capability in llms via reinforcement learning. *arXiv preprint arXiv:2501.12948*, 2025.
- Hou, W., Cheng, Y., Xu, K., Li, W., and Liu, J. RECAP: Towards precise radiology report generation via dynamic disease progression reasoning. In *Findings of the Association for Computational Linguistics: EMNLP 2023*, pp. 2134–2147. Association for Computational Linguistics, December 2023.
- Hu, E. J., Shen, Y., Wallis, P., Allen-Zhu, Z., Li, Y., Wang, S., Wang, L., Chen, W., et al. Lora: Low-rank adaptation of large language models. *ICLR*, 1(2):3, 2022.
- Irvin, J., Rajpurkar, P., Ko, M., Yu, Y., Ciurea-Ilcus, S., Chute, C., Marklund, H., Haghighi, B., Ball, R., Shpankaya, K., et al. Chexpert: A large chest radiograph dataset with uncertainty labels and expert comparison. In *Thirty-Third AAAI Conference on Artificial Intelligence*, 2019.

- Jin, H., Che, H., Lin, Y., and Chen, H. Promptmrg: Diagnosis-driven prompts for medical report generation. In *Proceedings of the AAAI Conference on Artificial Intelligence*, volume 38, pp. 2607–2615, 2024.
- Johnson, A. E., Pollard, T. J., Berkowitz, S. J., Greenbaum, N. R., Lungren, M. P., Deng, C.-y., Mark, R. G., and Horng, S. Mimic-cxr, a de-identified publicly available database of chest radiographs with free-text reports. *Scientific data*, 6(1):317, 2019.
- Lavie, A. and Agarwal, A. METEOR: An automatic metric for MT evaluation with high levels of correlation with human judgments. In *Proceedings of the Second Workshop on Statistical Machine Translation*, pp. 228–231. Association for Computational Linguistics, June 2007.
- Li, C., Wong, C., Zhang, S., Usuyama, N., Liu, H., Yang, J., Naumann, T., Poon, H., and Gao, J. Llava-med: Training a large language-and-vision assistant for biomedicine in one day. In *Advances in Neural Information Processing Systems*, volume 36, pp. 28541–28564. Curran Associates, Inc., 2023.
- Lin, C.-Y. Rouge: A package for automatic evaluation of summaries. In *Text summarization branches out*, pp. 74–81, 2004.
- Liu, F., Wu, X., Ge, S., Fan, W., and Zou, Y. Exploring and distilling posterior and prior knowledge for radiology report generation. In *Proceedings of the IEEE/CVF conference on computer vision and pattern recognition*, pp. 13753–13762, 2021a.
- Liu, F., Yin, C., Wu, X., Ge, S., Zhang, P., and Sun, X. Contrastive attention for automatic chest X-ray report generation. In *Findings of the Association for Computational Linguistics: ACL-IJCNLP 2021*, pp. 269–280, Online, August 2021b. Association for Computational Linguistics.
- Liu, H., Li, C., Li, Y., and Lee, Y. J. Improved baselines with visual instruction tuning. In *Proceedings of the IEEE/CVF Conference on Computer Vision and Pattern Recognition (CVPR)*, pp. 26296–26306, June 2024a.
- Liu, Z., Zhu, Z., Zheng, S., Zhao, Y., He, K., and Zhao, Y. From observation to concept: A flexible multi-view paradigm for medical report generation. *IEEE Transactions on Multimedia*, 26:5987–5995, 2024b.
- Liu, Z., Sun, Z., Zang, Y., Dong, X., Cao, Y., Duan, H., Lin, D., and Wang, J. Visual-rft: Visual reinforcement fine-tuning. *arXiv preprint arXiv:2503.01785*, 2025.
- Miura, Y., Zhang, Y., Tsai, E., Langlotz, C., and Jurafsky, D. Improving factual completeness and consistency of image-to-text radiology report generation. In *Proceedings of the 2021 Conference of the North American Chapter of the Association for Computational Linguistics: Human Language Technologies*, pp. 5288–5304. Association for Computational Linguistics, 2021.
- Nan, Y., Zhou, H., Xing, X., and Yang, G. Beyond the hype: A dispassionate look at vision-language models in medical scenario. *arXiv preprint arXiv:2408.08704*, 2024.
- Ostmeier, S., Xu, J., Chen, Z., Varma, M., Blankemeier, L., Bluethgen, C., Md, A. E. M., Moseley, M., Langlotz, C., Chaudhari, A. S., and Delbrouck, J.-B. GREEN: Generative radiology report evaluation and error notation. In *Findings of the Association for Computational Linguistics: EMNLP 2024*, pp. 374–390, Miami, Florida, USA, November 2024. Association for Computational Linguistics.
- Ouyang, L., Wu, J., Jiang, X., Almeida, D., Wainwright, C., Mishkin, P., Zhang, C., Agarwal, S., Slama, K., Ray, A., Schulman, J., Hilton, J., Kelton, F., Miller, L., Simens, M., Askell, A., Welinder, P., Christiano, P. F., Leike, J., and Lowe, R. Training language models to follow instructions with human feedback. In *Advances in Neural Information Processing Systems*, volume 35, pp. 27730–27744. Curran Associates, Inc., 2022.
- Pan, J., Liu, C., Wu, J., Liu, F., Zhu, J., Li, H. B., Chen, C., Ouyang, C., and Rueckert, D. Medvlm-r1: Incentivizing medical reasoning capability of vision-language models (vlms) via reinforcement learning. *arXiv preprint arXiv:2502.19634*, 2025.
- Papineni, K., Roukos, S., Ward, T., and Zhu, W.-J. Bleu: a method for automatic evaluation of machine translation. In *Proceedings of the 40th annual meeting of the Association for Computational Linguistics*, pp. 311–318, 2002.
- Qin, H. and Song, Y. Reinforced cross-modal alignment for radiology report generation. In *Findings of the Association for Computational Linguistics: ACL 2022*, pp. 448–458. Association for Computational Linguistics, May 2022.
- Rajpurkar, P. and Lungren, M. P. The current and future state of ai interpretation of medical images. *New England Journal of Medicine*, 388(21):1981–1990, 2023.
- Satia, I., Bashagha, S., Bibi, A., Ahmed, R., Mellor, S., and Zaman, F. Assessing the accuracy and certainty in interpreting chest x-rays in the medical division. *Clinical medicine*, 13(4):349–352, 2015.

- Sloan, P., Clatworthy, P., Simpson, E., and Mirmehdi, M. Automated radiology report generation: A review of recent advances. *IEEE Reviews in Biomedical Engineering*, 2024.
- Tang, Q., Xu, L., Wang, Y., Zheng, B., Lv, J., Zeng, X., and Li, W. Dual-modality visual feature flow for medical report generation. *Medical Image Analysis*, 101:103413, 2025.
- Tanida, T., Müller, P., Kaissis, G., and Rueckert, D. Interactive and explainable region-guided radiology report generation. In *Proceedings of the IEEE/CVF Conference on Computer Vision and Pattern Recognition*, pp. 7433–7442, 2023.
- Touvron, H., Martin, L., Stone, K., Albert, P., Almahairi, A., Babaei, Y., Bashlykov, N., Batra, S., Bhargava, P., Bhosale, S., et al. Llama 2: Open foundation and finetuned chat models. *arXiv preprint arXiv:2307.09288*, 2023.
- Wang, P., Bai, S., Tan, S., Wang, S., Fan, Z., Bai, J., Chen, K., Liu, X., et al. Qwen2-vl: Enhancing vision-language model’s perception of the world at any resolution. *arXiv preprint arXiv:2409.12191*, 2024.
- Wang, Z., Han, H., Wang, L., Li, X., and Zhou, L. Automated radiographic report generation purely on transformer: A multicriteria supervised approach. *IEEE Transactions on Medical Imaging*, 41(10):2803–2813, 2022a.
- Wang, Z., Tang, M., Wang, L., Li, X., and Zhou, L. A medical semantic-assisted transformer for radiographic report generation. In *International Conference on Medical Image Computing and Computer-Assisted Intervention*, pp. 655–664. Springer, 2022b.
- Wang, Z., Liu, L., Wang, L., and Zhou, L. R2gengpt: Radiology report generation with frozen llms. *Meta-Radiology*, 1(3):100033, 2023a.
- Wang, Z., Liu, L., Wang, L., and Zhou, L. Metransformer: Radiology report generation by transformer with multiple learnable expert tokens. In *Proceedings of the IEEE/CVF Conference on Computer Vision and Pattern Recognition*, pp. 11558–11567, 2023b.
- Wei, J., Wang, X., Schuurmans, D., Bosma, M., Xia, F., Chi, E., Le, Q. V., Zhou, D., et al. Chain-of-thought prompting elicits reasoning in large language models. *Advances in neural information processing systems*, 35:24824–24837, 2022.
- Yan, B. and Pei, M. Clinical-bert: Vision-language pre-training for radiograph diagnosis and reports generation. *Proceedings of the AAAI Conference on Artificial Intelligence*, 36(3):2982–2990, Jun. 2022.
- Yang, S., Wu, X., Ge, S., Zhou, S. K., and Xiao, L. Knowledge matters: Chest radiology report generation with general and specific knowledge. *Medical image analysis*, 80:102510, 2022.
- Yang, S., Wu, X., Ge, S., Zheng, Z., Zhou, S. K., and Xiao, L. Radiology report generation with a learned knowledge base and multi-modal alignment. *Medical Image Analysis*, 86:102798, 2023.
- Yang, Y., You, X., Zhang, K., Fu, Z., Wang, X., Ding, J., Sun, J., Yu, Z., Huang, Q., Han, W., and Yu, J. Spatio-temporal and retrieval-augmented modelling for chest x-ray report generation. *IEEE Transactions on Medical Imaging*, pp. 1–1, 2025.
- Zhang, B., Liu, Z., Cherry, C., and Firat, O. When scaling meets LLM finetuning: The effect of data, model and finetuning method. In *The Twelfth International Conference on Learning Representations*, 2024a.
- Zhang, K., Jiang, H., Zhang, J., Huang, Q., Fan, J., Yu, J., and Han, W. Semi-supervised medical report generation via graph-guided hybrid feature consistency. *IEEE Transactions on Multimedia*, 26:904–915, 2024b.
- Zhang, K., Yang, Y., Yu, J., Fan, J., Jiang, H., Huang, Q., and Han, W. Attribute prototype-guided iterative scene graph for explainable radiology report generation. *IEEE Transactions on Medical Imaging*, 2024c.
- Zhang, K., Zhou, R., Adhikarla, E., Yan, Z., Liu, Y., Yu, J., Liu, Z., Chen, X., Davison, B. D., Ren, H., et al. A generalist vision–language foundation model for diverse biomedical tasks. *Nature Medicine*, pp. 1–13, 2024d.
- Zhang, S., Dong, L., Li, X., Zhang, S., Sun, X., Wang, S., Li, J., Hu, R., Zhang, T., Wu, F., and Wang, G. Instruction tuning for large language models: A survey, 2024e.
- Zhang, Z., Lee, K., Deng, W., Zhou, H., Jin, Z., Huang, J., Gao, Z., Marshall, D. C., Fang, Y., and Yang, G. Gema-score: Granular explainable multi-agent score for radiology report evaluation. *arXiv preprint arXiv:2503.05347*, 2025.

## 6. Appendix

---

### Algorithm 1 BoxMed-RL Training Process

---

**Require:** X-ray Image  $I$ , CoT Annotations  $C$ , Prompt  $q$ , Bounding Boxes  $B_{gt}$ , Format  $t$ , Raw Report  $O$

**Ensure:** BoxMed-RL ( $\pi$ ) with reasoning and spatial grounding ability; Adapter ( $\pi_{\text{Adapter}}$ ) for fluent report generation

- 1: **Phase I: Pretraining**
- 2: *Step 1: Medical Concept Learning (MCL)*
- 3: BoxMed-RL( $\pi$ ) with initial parameters  $\theta$
- 4: **for**  $epoch = 0 \rightarrow epochs$  **do**
- 5:   Given X-ray Image  $I$ , Annotations  $C$
- 6:   Compute MCL loss:  $\mathcal{L}_{\text{MCL}}(\theta) \leftarrow (I, C, \pi_{\theta})$
- 7:   Update parameters:  $\theta' \leftarrow \arg \min \mathcal{L}_{\text{MCL}}(\theta)$
- 8: **end for**
- //  $\theta'$  is the updated parameters after MCL
- 9: *Step 2: Spatially Verifiable Reinforcement (SVR)*
- 10: **for**  $epoch = 0 \rightarrow epochs$  **do**
- 11:   Given prompt  $q$ , sample  $N$  responses
- 12:    $\{y_1, \dots, y_N\} \leftarrow (q, \pi_{\theta'})$
- 13:   **for all**  $y_i$  **do**
- 14:     Compute IoU reward:  $\mathcal{R}_{\text{IoU}}(q, y_i) \leftarrow \text{IoU}(q, y_i, B_{gt})$
- 15:     Reward Combination:  $R(q, y_i) \leftarrow \mathcal{R}_{\text{IoU}}(q, y_i) + \mathcal{R}_{\text{format}}(q, y_i, t)$
- 16:     Compute SVR Expectation:  $\mathbb{E}_{\text{SVR}}(\theta') \leftarrow R(q, y_i)$
- 17:     Update parameters:  $\theta'' \leftarrow \arg \max \mathbb{E}_{\text{SVR}}(\theta')$
- 18:   **end for**
- 19: **end for**
- //  $\theta''$  is parameters after Pretraining
- 20: **Phase II: Downstream Adapter**
- 21: Freeze  $\pi_{\theta''}$  and initialize Adapter  $\pi_{\text{Adapter}}$  with parameters  $\theta''$
- 22: **for**  $epoch = 0 \rightarrow epochs$  **do**
- 23:   Given X-ray Images  $I$ , Raw Reports  $O$
- 24:   Compute Adapter loss:  $\mathcal{L}_{\text{Adapter}}(\theta'') \leftarrow (I, O, \pi_{\text{Adapter}}(\theta''))$
- 25:   Update parameters:  $\hat{\theta} \leftarrow \arg \min \mathcal{L}_{\text{Adapter}}(\theta'')$
- 26: **end for**
- // Adapter's parameters updated as  $\hat{\theta}$
- 27: **return** BoxMed-RL( $\pi$ ) with parameters  $\theta''$  and Adapter( $\pi_{\text{Adapter}}$ ) with parameters  $\hat{\theta}$

---

## 7. Acknowledgment

Guang Yang was supported in part by the ERC IMI (101005122), the H2020 (952172), the MRC (MC/PC/21013), the Royal Society (IEC/NSFC/211235), the NVIDIA Academic Hardware Grant Program, the SABER project supported by Boehringer Ingelheim Ltd, NIHR Imperial Biomedical Research Centre (RDA01), The Wellcome Leap Dynamic resilience program (co-funded by Temasek Trust), UKRI guarantee funding for Horizon Europe MSCA Postdoctoral Fellowships (EP/Z002206/1), UKRI MRC Research Grant, TFS Research Grants (MR/U506710/1), and the UKRI Future Leaders Fellowship (MR/V023799/1).